DESIGN AND APPLICATION OF MULTIFUNCTIONAL PERFORMANCE TEST PLATFORM FOR SOIL-ENGAGING TILLAGE COMPONENTS
/
多功能触土耕作部件性能检测平台设计与应用

Zhiquan Sun[1)], Zhou Yang[2, 3)], Jieli Duan[*2)], Jun Li[2)]
[1)] Experimental Basis and Practical Training Centre, South China Agricultural University, Guangzhou / China;
[2)] College of Engineering, South China Agricultural University, Guangzhou / China;
[3)] Guangdong Provincial Key Laboratory of Conservation and Precision Utilization of Characteristic Agricultural Resources in Mountainous Areas, Meizhou / China
Tel: +86 02085280783; E-mail: duanjieli@scau.edu.cn
DOI: https://doi.org/10.356.33/inmateh-62-37

Keywords: *tillage components, multifunctional, test platform, soil-engaging*

ABSTRACT
Parts that come into contact with the soil are ones of the important energy consuming parts in tillage operations. In order to improve the research and development efficiency of tillage components, it is necessary to develop a performance test platform for tillage components with high interchangeability, convenience and comprehensive data collection. Therefore, a performance test platform for combined powered and passive tillage components was designed. Strength analysis and structural design optimization of key components was based on ANSYS. A real-time measurement and control software was developed based on LabVIEW platform. The related tests results show that the test platform can be used to simulate the actual condition and meet the test requirements.

摘要
在耕作作业中，触土部件是耕作机械重要耗能部件之一。为提高耕作部件的研发效率，需研制具有较高互换性、便捷性和数据采集全面的耕作部件性能检测平台，本文研发了同时适用于主动和被动耕作部件的小型性能测试平台，基于 ANSYS 对关键部件进行强度分析和结构设计优化，开发了基于 LabVIEW 平台的实时测控软件。利用所研发的测试平台，对双翼铲和微耕刀工作性能进行试验分析。研究结果表明：1）检测平台可实时调整耕作部件工作参数并在线采集、显示与存储试验数据；2）检测平台可测试被动耕作部件耕深范围为 0 ~ 400mm；对于主动开沟部件，可检测的耕深范围为 0 ~350 mm、转速在 100 ~700 r/min 之间；3）双翼铲开沟器前进阻力、竖直方向阻力及侧向阻力与行进速度成正比，且侧向阻力远大于其它两方向阻力，旋转圆盘开沟器工作扭矩与前进速度成正比，所设计检测平台能够模拟实际工况，满足试验要求。

INTRODUCTION

The energy consumption of tillage machinery accounts for more than 50% of the energy consumption of field operations, and the soil contact resistance of tillage part is one of the important factors in the energy consumption *(Zhijun Guo et al., 2011)*. Therefore, the interaction characteristics between tillage part and soil during the tillage operations is of great significance for optimizing the design of tillage machinery, improving tillage efficiency, saving energy, and reducing emissions, thus promoting the process of agricultural mechanization in China *(Honglei Jia et al., 2017)*. At present, the researches on tillage components mainly focus on the simulation of the soil-touching process and the work effect in the field of the tillage machinery. However, there are obvious differences between the actual situation and the ideal simulated test conditions, so simulation studies need to be tested and verified *(Shoutai Li et al., 2011; Huimin Fang et al., 2016)*. The field detection is usually applied to test the performance of the complete machine, which is limited by environment and electric power, so the detection accuracy is low and the data collection is difficult. Test platform with the characteristics of controllable soil factors, make easy recovery of soil state, easy debugging of test equipment and repetitive test results. The indoor test platform is not affected by seasons or weather *(Yonglei Li et al., 2012)*, so the indoor test platform is the developing direction in future.

The United Kingdom, Germany, France, the United States, Canada, Israel and other countries have started indoor test platform research earlier, and have reached a fairly high level of automation *(Ani et al.,2018;*

Hemmat et al., 2014). China's indoor test platform is mainly large-scale type, which is mainly used to test the performance and work effect of rotary tillers, micro-farming machine and other complete machines *(Weixing Wang et al., 1997; Hua Yan et al., 2010; Xincheng Sun et al 2015; Yan Yu et al., 2011)*. Currently existing small test platforms are mostly used to test the performance of passive tillage component, the test object and mode are single *(Yanjie Li et al., 2010; Jianneng Chen et al., 2015)*. Furthermore, low universality and interchangeability of the small test platform also limit the testing and development of tillage components. Therefore, it is very important to develop a test platform which is suitable for a variety of tillage components.

In this paper, a multifunctional test platform was designed and can be used for the testing of passive tillage equipment such as plough and powered tillage equipment such as rotary tiller blades, chain ditcher or vertical spiral ditcher. The small sized and interchangeable test platform has advantages such as having wide in application range, being accurate in data acquisition and efficient in testing.

MATERIALS AND METHODS

Overall structure of test platform

The overall structure diagram of the test platform is shown in Fig. 1. The test platform consists of four parts: traction drive system, soil box, tillage equipment drive system and test platform measurement and control system. The traction system drives the wire ropes to move the trolley on the straight track. The tillage equipment drive system is mounted on the trolley, and the trolley guide wheel device is designed to ensure the trolley to run straight and avoid friction with the track. The motor drives the rotary tillage equipment to work. A LabVIEW-based measurement and control system is developed to adjust the working performance of the tillage equipment and collect test data in real time online.

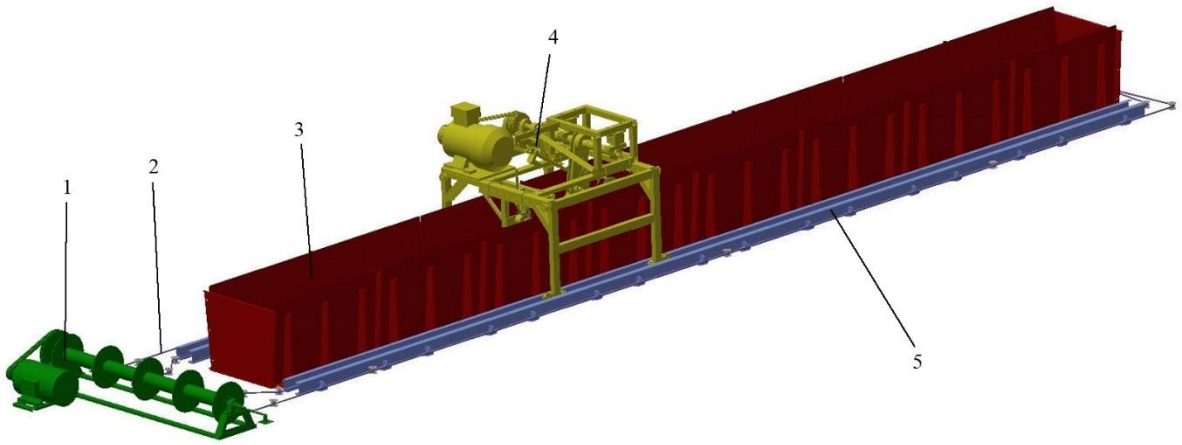

Fig. 1 - General model of test platform

1 – Traction drive system; 2 – Steel wire rope; 3 – Soil box; 4 – Tillage equipment drive system; 5 – Track

Table 1

Performance parameters of the trolley

Tillage components	Maximum drive power	Deceleration ratio	Speed range	Depth range of ploughing
	[kW]		[rpm]	[mm]
Powered	15	1.57	200~700	0~350
		3	100~460	
Passive	4			0~400

Tillage trolley

The parameters of the trolley are listed in Table 1 *(Yanshan Yang et al., 2016; Zhou Yang et al., 2013; Wenfeng Ji, 2010)*. In order to improve the universality of the test platform and meet the test requirements of different tillage modes and tillage equipment, a multifunctional test trolley is designed (in Fig. 2) *(Jianguo Zhao et al., 2019; Kan Zheng et al., 2017)*.

The tillage drive system is the main working part of the test platform, which can be used to detect the powered tillage equipment, the passive tillage equipment and the powered-passive combination tillage equipment *(Chinese Academy of Agricultural Mechanization Sciences, 2007)*. The main body of the tillage drive system is mounted on the trolley.

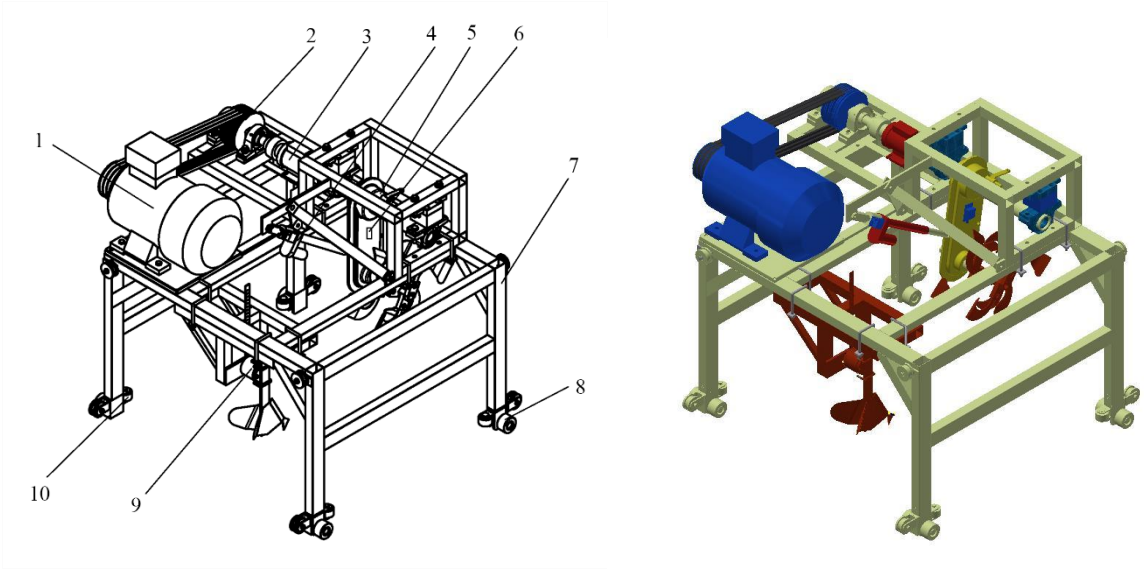

Fig. 2 - Integral design of tillage trolley

1 – Motor; 2 – Pulley; 3 – testing device for powered tillage components; 4 – Frame; 5 – Road wheel; 6 – Testing device for passive tillage components 7 – sheave

Key component design

Soil factors have a great influence on the performance of tillage machines and tools (*Bashar M et al., 2015*). In order to ensure that the soil box has enough strength, the ANSYS software is used to analyse the stress on the soil box and optimize the structural design. When compacting the soil, the stress on the sidewall of the soil box is greatest. From the foundation soil stress theory of generalized Hooke's law, soil physical property measurement and calculation method *(Caihong Jia, 2013)*, lateral stress of soil on the inner wall soil, bulk density and soil gravity are calculated by the following equations.

$$p = k_0(\gamma z + \sigma_c) \text{ [kPa]} \quad (1)$$

$$rs = \frac{m_0}{V(1+0.01w_0)} \text{ [g/cm}^3\text{]} \quad (2)$$

$$\gamma = \frac{rs \cdot g}{1000} \text{ [kN/m}^3\text{]} \quad (3)$$

where:

p is the lateral static soil stress; γ is the fill weight; z is the calculated point depth; k_0 is the lateral pressure coefficient; σ_c is the additional stress; rs is the soil bulk density; m_0 is the quality of the model wet soil; V is the volume of the ring cutter; w_0 is the moisture content of the soil sample; g is the acceleration of gravity.

In addition, the Boussinesq's formula *(Caihong Jia, 2013)* establishes a three-dimensional coordinate system with the base point of the rectangular load as the origin, and the additional stress at any depth z under the base corner point:

$$\sigma_z = \frac{3p_0}{2\pi}\int_0^l\int_0^b \frac{z^3 dxdy}{(x^2+y^2+z^2)^{5/2}} \text{ [MPa]} \quad (4)$$

where:

p_0 is the load strength; σ_z is the additional stress at depth z;

l is the load length;

b is the load width.

The integral result of equation (4) is:

$$\sigma_z = \alpha_c p_0 \text{ [MPa]} \quad (5)$$

The soil gravity parameter in equation (1) is consistent with the soil bulk density parameter (*Jia Caihong, 2013*), and σ_c is substituted into equations (2), (3), and (5) with σ_z to obtain equation (6).

$$p = k_0\left(\frac{m_0 g}{V(1000+10w_0)}z + \alpha_c p_0\right) \text{ [MPa]} \quad (6)$$

When the compaction wheel compacts the soil, the stress distribution is roughly elliptical. The maximum vertical stress is distributed on the axle vertical line. The vertical stress decreasing from top to bottom and decreasing from the axle vertical line to both sides along the advancing direction *(Zhenjia Zhao et al., 2012; Ruxin Li et al., 2001)*. Due to the complex stress variation during compaction of the soil, it is difficult to detect accurately. The elliptical surface is divided into three internal stress zones according to the stress distribution trend. Each area is divided into three parts: left, centre and right. Vertical stress distribution is shown in Fig. 3.

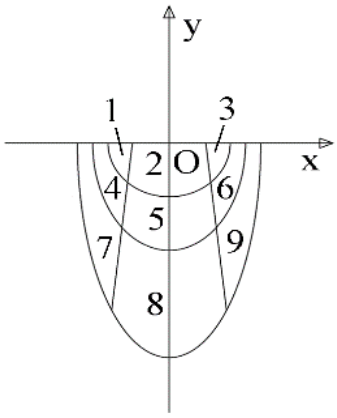

Fig. 3 - Soil vertical stress distribution

In order to improve the feasibility of the simulation and make it as possible as close to the actual conditions, the central stress of each block is taken as the plane stress of this block. The soil bulk density was measured using a standard soil wreath knife with a volume of 60 cm^3 and soil hardness was measured by a serpentine sampling method *(Nanjing Hydraulic Research Institute, 2003)*.

The measurement site is the citrus orchard of the Institute of Fruit Research, Guangdong Academy of Agricultural Sciences. The measured soil wet weight m_0=100.6 g, soil moisture content w_0=13.3%, and soil firmness are listed in Table 2.

Table 2

Soil parameter of the citrus orchard of the Institute of Fruit Research, Guangdong Academy of Agricultural Sciences

Depth	Soil firmness													Average value
[cm]	[kPa]													[kPa]
60	241	245	231	262	380	352	293	145	153	146	250	203	418	255.31
120	272	331	335	362	401	370	303	195	159	137	361	333	399	304.46
180	29	346	458	424	469	446	376	172	121	243	401	384	474	354.38
240	273	415	469	387	464	502	449	289	326	357	441	430	487	406.85
300	411	461	482	452	443	541	483	299	319	460	428	462	438	436.85
360	431	456	467	452	582	514	514	281	426	448	428	475	405	452.23

According to the measured soil parameters, take k_0=0.5, g=9.81 N/kg, p_0=350 kPa. According to surface length l=400 mm, width b=200mm, look up the table to get the value of σ_c. Substituting the values into the equation (6), the results are listed in Table 3 *(Chunlin Li, 2009)*. Consider the symmetry relationship of stress distribution, the results of only one side stress are listed in Table 3. The material used is Q235 steel plate, the allowable stress is 156.67 MPa (safety factor is 1.5).

In order to facilitate loading the stress, the load plate covering the inner side wall of the soil box is designed according to the stress region division aforementioned. The material selection unit is type SOLID187, Poisson's ratio is 0.3, elastic modulus is 2.06×105 MPa, density is 7800 kg/m^3. The model adopts automatic mesh division in the process of simulation. Stress load is applied on the load plate and stress intensity analysis based on the third strength theory is performed. It is necessary to optimize the design of the soil box to ensure the safety and reliability of test platform.

Generally, increasing the thickness of the steel plate or increasing the sidewall ribs can reinforce the soil box. So the simulation calculation method is used to determine the thickness of the steel plate that meets the strength requirements. Two designs are simulated with a gradient of 0.5 mm of steel plate. The results are listed in Table 5.

The soil box without ribs needs 8.5 mm thick steel plate, 9mm thick steel plate is used in the actual condition. The 2mm thick steel plate with grooved ribs can meet the requirements. Due to the harsh working environment of the tillage equipment, the soil box with grooved ribs is finally designed to use 3mm plates. Under the premise of meeting the safety and reliability of the test platform, the ribbed soil box will save 52.19% of material compared to the non-ribbed soil box. The stress cloud diagram of soil box is shown in Fig. 4, the maximum stress of the soil box with grooved ribs is 124.06MPa, and the maximum displacement is 0.18mm.

Table 3

Stress values at different locations

Load point	x	y	Stress coefficient	Horizontal stress [MPa]
1	-85	-30	0.235	0.076
2	0	-50	0.239	0.084
4	-100	-70	0.226	0.040
5	0	-150	0.166	0.058
7	-110	-160	0.226	0.040
8	0	-300	0.093	0.033

Table 4

Simulation calculation result of two designs

Type of soil box	Thickness of steel plate	Maximum stress	Maximum displacement	Meet the conditions
	[mm]	[MPa]	[mm]	
non-ribbed	8	204.07	4.75	NO
	8.5	138.99	4.01	YES
	9	120.48	3.41	YES
grooved ribs	1.5	170.87	0.44	NO
	2	142.12	0.30	YES

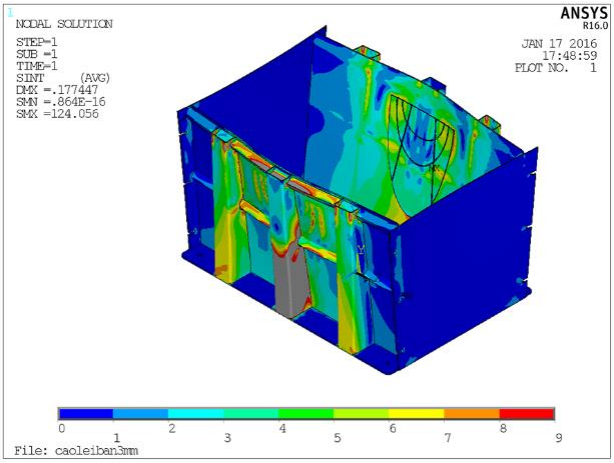

Fig. 4 - ANSYS stress cloud diagram of 3 mm thick steel plate soil box with grooved ribs

Measurement and control system design

Measurement and control system hardware design

The measurement and control system consists of the host computer, the lower computer and the actuator. The parameters of the torque, rotation speed, tillage depth and three-dimensional resistance of passive tillage equipment and forward speed of the trolley can be detected and displayed in real time. The sensor is used to convert the physical phenomena to a standard voltage signal.

The signal is collected by the data acquisition card and then processed and displayed by the test platform. The data is collected by two data acquisition cards (PCI-1706U and USB-4711A), which were produced by Advantech. The lower computer 1 and 2 adopts Shanghai Hongqitai RF300A15kW and Siemens M4407.5kW inverter, as the controller of traction drive system and tillage drive system, respectively, controls the inverter through the analogue and digital output ports of the acquisition card; adopts STC89C52RC MCU as the lower computer 3, based on the VISA driver of LabVIEW, the RS232 serial communication is used to establish the master-slave relationship between the PC and the MCU. The MCU controls the electric push rod to adjust tillage depth *(Shun Xu et al., 2017; Bin Xie et al., 2013)*. The structure of measurement and control system hardware is shown in Fig. 5.

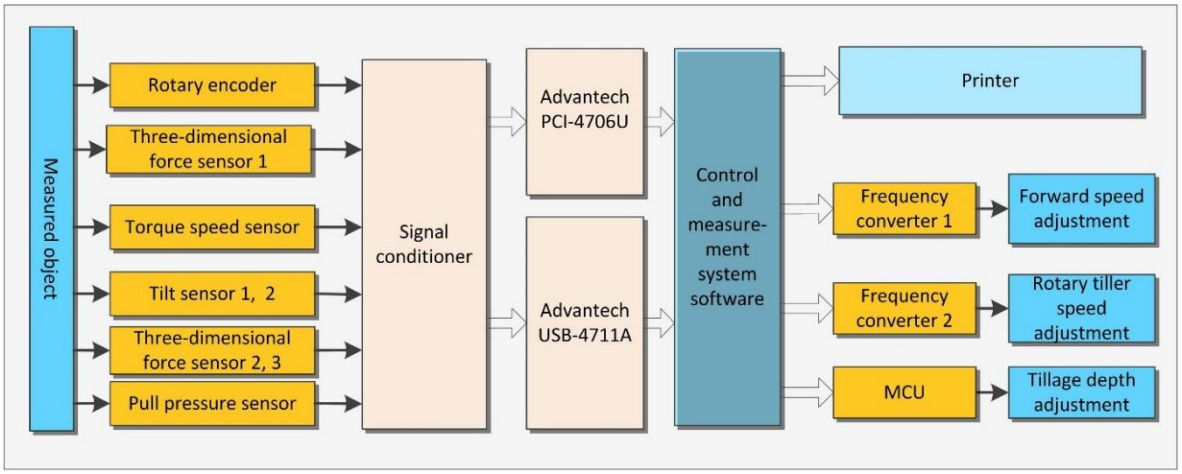

Fig. 5 - Overall structure of the measurement and control system

Measurement and control system software design

Based on the LabVIEW platform, the measurement and control software for the test platform is developed *(Chunlin Xu et al., 2013)*. The software can fulfil the requirements of test parameter adjustment, real-time data display and storage, with a friendly operation interface and strong human-computer interaction. The software includes four tabs: system calibration, test platform control, passive tillage equipment test, and powered tillage equipment test. The calibration program is used to select the COM port that communicates the host computer with the MCU, and mark θ_0. When no load occurs torque magnitude is marked. The system realizes the functions of adjusting the direction and speed of the trolley, controlling the steering and rotating speed of the powered tillage equipment and saving the data. The human-computer dialogue of the software is shown in Fig. 6.

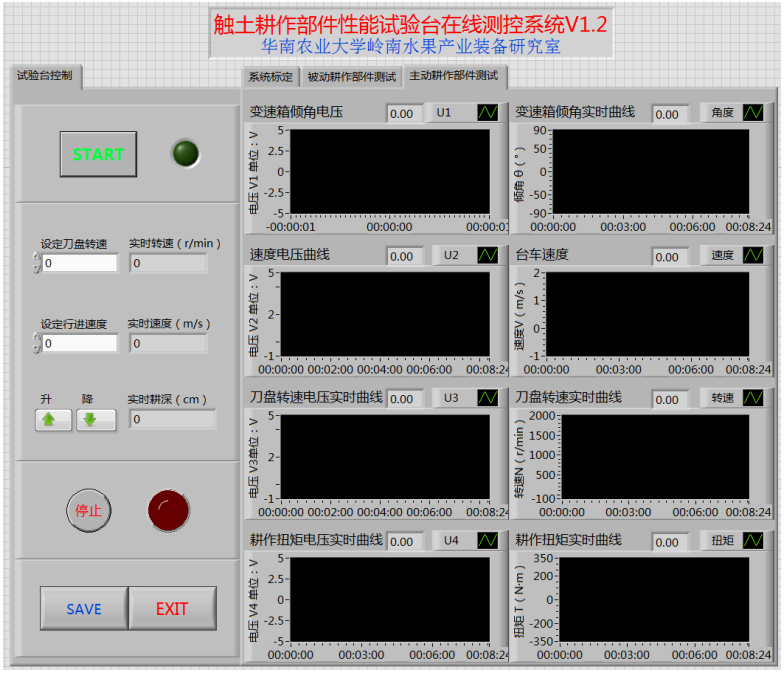

Fig. 6 - LabVIEW-based measurement and control system software

RESULTS

The tillage equipment is mounted on the corresponding detection device as shown in Fig. 7. Double shovel plough width B=70 mm, penetration angle α<90°. Micro rotary tiller blades bending radius is R=30 mm, bending angle φ=120°, width B1=42 mm, slip angle γ=30°, as shown in Fig. 8. A single factor test was designed with the tillage depth being 100 mm, the blades rotation speed 320 r/min, the forward speed of 0.1, 0.2, and 0.3 m/s.

Fig. 7 - The test platform

(a) **(b)**

Fig. 8 - Double shovel plough and micro rotary tiller blades assembly

As shown in Fig. 9 and Fig. 10, when the forward speed increases from 0.1 m/s to 0.2 m/s under the condition of 100 mm tillage depth, the average forward resistance (Fx) of the double shovel plough opener increases from 70.43N to 143.01N, an increase of 50.75%. The average resistance in the vertical direction (Fy) increased from 121.09N to 256.98N, an increase of 52.88%, the lateral average resistance (Fz) increased from 853.70N to 1166.81N, an increase of 26.83%; the forward speed increased from 0.2m/s to 0.3m/s, Fx increased from 143.01N to 211.64N, an increase of 32.43%, Fy from 256.98N to 362.46N, an increase of 29.10%, Fz from 1166.81N to 1389.15N, an increase of 16.01%. The three-dimensional resistance of the double shovel plough is proportional to the forward speed, but the three-dimensional resistance increases slowly as the speed increases.

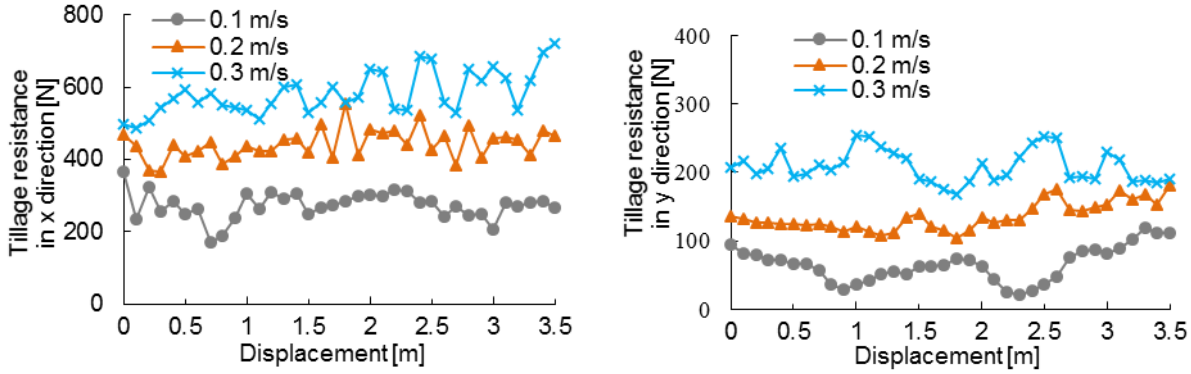

(a) **(b)**

Fig. 9 – Tillage resistances of double shovel plough in X and Y directions

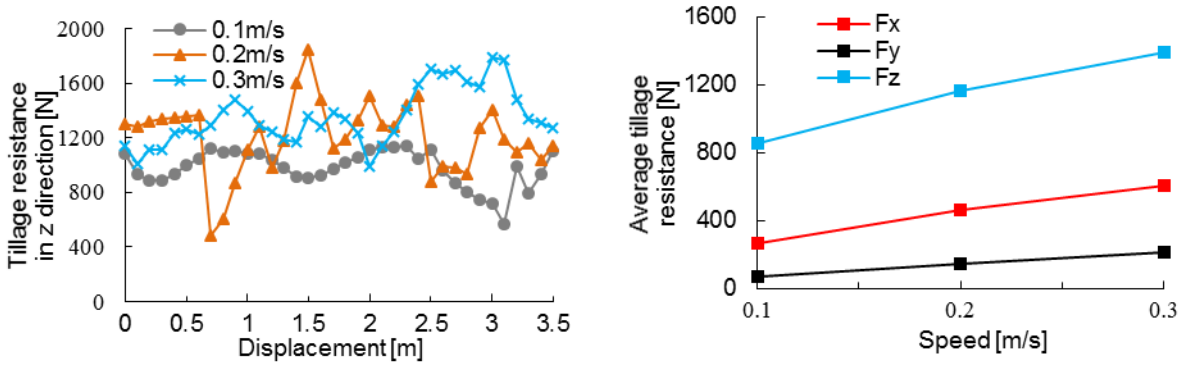

(a) (b)

Fig. 10 – Tillage resistance of double shovel plough in z direction and average resistance in x, y and z directions

It can be seen from Fig. 10(b) that the lateral resistance Fz is much larger than the other two directions. This is because the central symmetry plane of the double shovel plough has a certain angle with the advancing direction during installation or the two sides of the shovel are not symmetrical during the manufacturing process. Therefore, the passive equipment devices such as the double shovel plough have high accuracy on manufacturing and assembly, otherwise there will be greater additional resistance and will lead to affect machine life. Fig. 11 shows the test result of micro rotary tiller blades. When the forward speed increases from 0.1 m/s to 0.2 m/s, the average working torque (T) of the cutter head increases from 12.90 nm to 22.10 nm, an increase of 41.64%. When the forward speed increases from 0.2 m/s to 0.3 m/s, it increases from 22.10 nm to 27.97 nm, an increase of 20.99%, and the working torque of the micro rotary tiller blades is proportional to the forward speed under the conditions of 100 mm of tillage depth and 320 rpm of rotation speed, but the working torque increases slowly with the forward speed increasing. The test platform can effectively simulate the field soil and the working conditions of the tillage equipment in different modes. The test platform is highly interchangeable, and the performance parameters of different types of tillage equipment can be effectively collected.

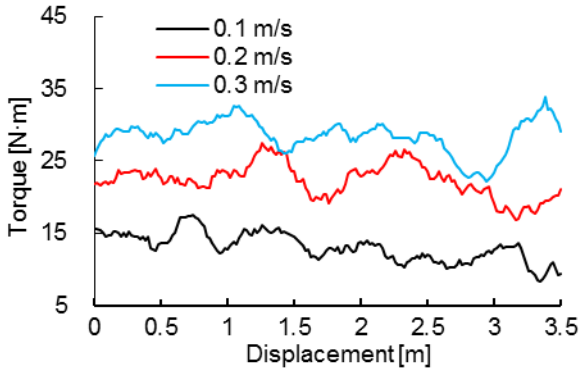

Fig. 11 - Working torque of micro rotary tiller blades

CONCLUSIONS

1) The multi-mode tillage equipment test platform can test the passive tillage components at a depth of 0~400 mm, and test the powered tillage equipment with a depth of 0~350 mm at speed of 100~700 rpm. The test platform has the characteristics of small floor area, movable, strong comprehensiveness and high interchangeability. It can be used for a variety of tillage equipment and multiple tillage modes, thereby reducing the research and development cost of tillage equipment and improving the development efficiency.

2) The measurement and control system software is developed based on the LabVIEW platform, which can adjust the forward speed of the tillage equipment, the tillage depth, the blades rotation speed in real time. The test data such as the forward speed, the working torque and the rotation speed of the blades, and the three-dimensional tillage resistance of the passive tillage equipment are displayed in real time online and stored by the software. The software improves the automation of the test platform, and is convenient to use and easy to operate.

3) Based on the soil mechanics theory and ANSYS simulation, the design and optimization of the soil box is carried out. The simulation results show that the grooved rib soil box saves 52.19% of material compared with the non-ribbed soil box under the condition of meeting the strength requirement. The design method and simulation result can provide a reference for the design of soil box.

4) The test results of the double shovel plough and the micro tiller blades indicate that the forward resistance, the vertical resistance and the lateral resistance of the double shovel plough are all proportional to the advancing speed, and the three-dimensional resistance increases slower when the speed increases. The working torque of the micro tiller blades is proportional to advancing speed, and the torque increases slower when the speed increases. The designed test platform can simulate the actual condition and meet the actual work needs.

ACKNOWLEDGEMENT

This work was supported by Key-Area Research and Development Program of Guangdong Province (2019B020223002), Natural Science Foundation of Guangdong Province (2020A1515010793), and National Banana Industry Technology System Construction Project of China (CARS-31-10).

REFERENCES

[1] Ani O.A., Uzoejinwa B.B., Ezeama A.O., Onwualu A.P., Ugwu S.N., Ohagwu C.J. (2018). Overview of soil-machine interaction studies in soil bins. *Soil and Tillage Research*, *USA*, 175, 13-27. https://doi.org/10.1016/j.still.2017.08.002

[2] Chen J. N., Ye J., Xia X. D., Zhao Y. (2015). Design and application of rotary round soil-bin test bed driven by tyre friction. *Transactions of the Chinese Society of Agricultural Machinery*, 46(7), 66-71. http://www.en.cnki.com.cn/Article_en/CJFDTotal-NYJX201507010.htm

[3] China Academy of Agricultural Mechanization Science, (2007). Design manual of agricultural machinery. Issue I, *China Agricultural Science and Technology Press*, *China*, 75-259.

[4] Fang H. M., Ji C. Y., Zhang Q. Y., Guo J. (2016). Force analysis of rotary blade based on distinct element method. *Transactions of the CSAE*, 32(21), 54-59. http://www.en.cnki.com.cn/Article_en/CJFDTOTAL-NYGU201621007.htm

[5] Guo Z. J., Du G., Zhou Z. L., Zhang P., Li Y. X. (2011). Actuality analysis of resistance-reducing properties on soil cultivating components with different macroscopic soil-engaging surfaces. *Transactions of the Chinese Society of Agricultural Machinery*, 42(6), 47-52. https://www.researchgate.net/publication/288996856

[6] Hemmat A., Rahnama T., Vahabi Z. (2014). A horizontal multiple-tip penetrometer for on-the-go soil mechanical resistance and acoustic failure mode detection. *Soil and Tillage Research*, *USA*, 138, 17-25. https://doi.org/10.1016/j.still.2013.12.003

[7] Ji W. F., Jia H. L., Tong J., Tan H. J., Liu Z.C., Ma C. L. (2010). Analysis of influencing factors on power consumption and field test of universal blade. *Transactions of the Chinese Society of Agricultural Machinery*, *China*, 41(2), 35-41. https://www.researchgate.net/publication/289204345

[8] Jia C. H. (2013). Soil mechanics. *Peking University Press*, 53-67.

[9] Jia H. L., Wang W. P., Chen Z., Zhang T. Z., Zhang P., Zhuang J. (2017). Research status and prospect of soil-engaging components optimization for agricultural machinery. *Transactions of the Chinese Society of Agricultural Machinery*, 48(7), 1-13. http://en.cnki.com.cn/Article_en/CJFDTOTAL-NYJX201707001.htm

[10] Li C. L. (2009). Stress behaviour in agricultural soil compacting process and the development and application of its monitoring system. *Nanjing Agricultural University*, 7-9. DOI:10.7666/d.Y1762838

[11] Li S. T., Chen X. B., Chen W., Zhu S.P., Li Y. W., Yang L., Xie S. Y. (2018). Soil-cutting simulation and parameter optimization of handheld tiller's rotary blade by smoothed particle hydrodynamics modelling and Taguchi method. *Journal of Cleaner Production*, *USA*, (179), 55-62. https://www.sciencedirect.com/science/article/pii/S0959652617332183

[12] Li Y. J., Xu Y., Zhao D. (2010). Development and manufacture of a mini-soil-bin device for soil dynamics experiments. *Journal of Mechanical Engineering*, 46(15), 65-70. https://en.cnki.com.cn/Article_en/CJFDTOTAL-JXXB201015028.htm

[13] Li Y. L., Song J. N., Dong X. Q., Zhang J. K., & Wang J. C. (2012). Design of test device for rotary tiller components based on soil bin. *Transactions of the CSAE*, 28(17), 38-43

http://en.cnki.com.cn/Article_en/CJFDTOTAL-NYGU201217008.htm
[14] Li R. X., Song H. B., & Gao H. W. (2001). Prediction of soil compaction by small tractor using finite element method. *Transactions of the CSAE*, 17(4), 66-69. http://www.en.cnki.com.cn/Article_en/CJFDTOTAL-NYGU200104016.htm
[15] Nanjing Hydraulic Research Institute. (2003). Technical manual of geotechnical test. *Communication Press*, *China*, 34-35.
[16] Sun X. C., Ye J., Yan J. J., Chen J. N. (2015). Running stability control method and test verification of soil groove test rig for rotary agricultural machine. *Transactions of the CSAE*, 31(13), 46-52. https://www.researchgate.net/publication/282903191
[17] Taghavifar, H., Mardani, A. (2014), Analyses of energy dissipation of run-off-road wheeled vehicles utilizing controlled soil bin facility environment. *England*, 66, 973-980. https://doi.org/10.1016/j.energy.2014.01.076
[18] Wang W. X., Luo X. W., Ou Y. G., & Luo X. W. (1997). Research on computerized simulation loading system for soil trough tests. *Transactions of the CSAE*, 13(4), 27-30. http://www.tcsae.org/nygcxb/ch/reader/view_abstract.aspx?file_no=19970406
[19] Xie B., Li H., & Zhu Z. X. (2013). Measuring tillage depth for tractor implement automatic using inclinometer. *Transactions of the CSAE*, 29(4), 16-21. https://www.researchgate.net/publication/289213268
[20] Xu C. L., Li L. H., Zhao D. Y., Li X. Q., Li M. J., & Zhang W. (2013). Field real time testing system for measuring work dynamic parameters of suspension agricultural implement. *Transactions of the Chinese Society of Agricultural Machinery*, *CHINA*, 44(4), 82-88. https://www.researchgate.net/publication/289319964
[21] Xu S., Tong J., & Li M. (2017). Performance testing of vegetable chopping machine based on LabVIEW and operation parameter optimization. *Transactions of the CSAE*, *CHINA*, 33(3), 250-256. https://www.researchgate.net/publication/316254466
[22] Yan H., Wu J. M., & Lin J. T. (2010). Design of micro-cultivator or testing platform with annular soil bin. *Transactions of the Chinese Society of Agricultural Machinery*, S1(41), 68-72. http://en.cnki.com.cn/Article_en/CJFDTOTAL-NYJX2010S1016.htm
[23] Yang Y. S., Ding Q. S., Ding W. M., Xue J. L., Qiu W., & He R. Y. (2016). Design and application of multi-purpose in-situ tillage tool testing platform. *Transactions of the Chinese Society of Agricultural Machinery*, 47(1), 68-74. https://www.researchgate.net/publication/298714193
[24] Yang Z., Chen C. H., Duan J. L., Yan G. Q., Pan X. W., Yan L. L., & Liu J. L. (2013). Performance test of hand-held electric hole-digger for fertilization in orchard. *Transactions of the CSAE*, 29(12), 25-31. https://www.researchgate.net/publication/289176183
[25] Yu Y., Gong L. N., & Shang S. Q. (2011). Development of soil bin test dynamic parameters measurement system. *Transactions of the CSAE*, 27(S1), 323-328. https://www.researchgate.net/publication/291289304
[26] Zhao J. G., Wang A., Ma Y. J., Li J. C., Hao J. J., Nie Q. L, Long S. F., & Yang Q. F. (2019). Design and test of soil preparation machine combined subsoiling, rotary tillage and soil breaking. *Transactions of the CSAE,* 35(8), 46-54. https://en.cnki.com.cn/Article_en/CJFDTotal-NYGU201908006.htm
[27] Zhao Z. J., Zou M., Xue L., Wei, C. G., & Li J. Q. (2012). Simulation analysis of effect of compaction on soil stress distribution. *Transactions of the Chinese Society of Agricultural Machinery*, 43(S1), 311-313. https://www.researchgate.net/publication/289056143
[28] Zheng K., He J., Li H. W., Zhao H. B., Hu H. N., & Liu W. Z. (2017). Design and experiment of combined tillage implement of reverse-rotary and subsoiling. *Transactions of the Chinese Society of Agricultural Machinery*, 48(8), 61-71. https://www.researchgate.net/publication/320430124